Shear Dispersion and Error Decay in Idealized Twin Experiments

MEI-MAN LEE

James Rennell Division, Southampton Oceanography Centre, Southampton, United Kingdom

(Manuscript received 30 October 2000, in final form 21 May 2001)

ABSTRACT

In understanding how errors decay in twin experiments, previous studies have shown that it can be due to bottom friction or geostrophic adjustment. However, there are quantities, such as passive tracers, that may not be recovered by either of these mechanisms. This study seeks a mechanism that can cause errors to decay in the absence of bottom friction or geostrophic adjustment.

Consider the particular case of an isopycnic layer where the velocity is perfectly known but the layer thickness is not. It will be argued that the errors in layer thickness decay by processes similar to that of tracer homogenization. Based on the fact that the homogenization is achieved by an initial rapid shear dispersion, it is hypothesized that the error decay is initially by shear dispersion. This hypothesis is tested using idealized twin experiments based on an eddy-resolving isopycnic channel model. A series of experiments with different diffusivities supports the idea that the initial decay timescale approximates to the shear dispersion timescale.

1. Introduction

Data assimilation provides a means of blending observational data with ocean models, in the hope of filling the gaps in observation and improving our understanding of the ocean. Before applying them to realistic models with real data, assimilation methods can be tested in twin experiments. These use two runs: a control run, representing a ''true'' state, and an assimilation run, representing a ''predicted'' state. The assimilation run is initialized with a condition different from the truth and is assimilated with some but not all quantities observed from the control run. For example, sea surface height or surface velocity are often assimilated since in the ocean these are well observed from satellite altimeters. The success of the assimilation is then judged by how well the predicted state converges to the true state.

Because twin experiments often assume perfect models, accurate data, etc., the convergence in these experiments may not be equivalent to that in realistic assimilation. However, twin experiments are useful in that they focus on the understanding of convergence processes and so give insights into why convergence occurs.

Berry and Marshall (1989) showed, in a two-layer quasigeostrophic model, that, if the top-layer streamfunction is reinitialized, the bottom-layer streamfunction is recovered by bottom friction. This is due to the damping of vorticity errors at an *e*-folding timescale inverse to the bottom friction coefficient. However, in a three-layer model, reinitializing the top-layer streamfunction introduces potential vorticity anomalies in the middle layer where the potential vorticity is otherwise homogenized (Haines 1991). Since the vorticity errors in the middle layer cannot be damped by bottom friction, this causes the errors in both the middle and the bottom layer to converge at a slower rate than in the two-layer case.

Haines et al. (1993) argued, in a three-layer shallow water model, that, by ''nudging'' the surface velocity field toward the truth, the layer thickness is altered through geostrophic adjustment on a timescale of $1/f$ (f is the Coriolis parameter). They also showed that imposing the constraint of no changes of potential vorticity in the deeper layers has a similar effect to the nudging method. However, not all quantities can be recovered by geostrophic adjustment. For example, temperature, salinity, and biogeochemical tracers on isopycnals have no direct feedback on the velocity field and thus play no active role in geostrophic adjustment. It seems unlikely that the advection of tracers by the gravity waves that mediate geostrophic adjustment should cause tracer errors to decay.

This study shows the operation of shear dispersion as a mechanism for error decay in the absence of bottom friction or geostrophic adjustment. The approach taken is as follows. Consider an isopycnic layer where the true velocity field is perfectly known. The predicted layer thickness, starting from an in-

Corresponding author address: Dr. Mei-Man Lee, James Rennell Division, Southampton Oceanography Centre, Southampton, SO14 3ZH, United Kingdom.
E-mail: mmlee@soc.soton.ac.uk

correct initial field, is then simply advected by the true velocity field. This treats the predicted layer thickness as passive in the sense that it has no feedback to the true velocity and hence geostrophic adjustment is excluded from this study.

Such a ''passive'' approach is perhaps not practical for realistic assimilation since the shear dispersion timescale is in general longer than the geostrophic adjustment timescale. However, it may serve as a baseline against which the success of assimilation methods that use nonpassive approaches can be judged.

The outline of the paper is as follows. Section 2 shows that the error between the true and predicted layer thickness fields behaves in a similar way to conserved tracers. A well-known property of conserved tracers is that they are homogenized by turbulent flows and the homogenization is achieved by an initial shear dispersion, followed by diffusion (Rhines and Young 1983). From this, it is hypothesized that the initial error decay is by shear dispersion. This is tested using a series of twin experiments. Section 3 describes the model, an eddy-resolving three-layer isopycnic model in a channel configuration. Section 4 gives the results and section 5 contains the discussion.

2. Background

a. Convergence

Suppose that the true ocean satisfies the continuity equation,

$$\frac{\partial h}{\partial t} + \nabla \cdot (\mathbf{u}h) = B + D, \tag{2.1}$$

where $\mathbf{u} = (u, v)$ is the horizontal velocity, h is the isopycnic layer thickness, B is the forcing, and D is the diffusion.

Consider an idealized situation where the velocity and the forcing are known, then the predicted layer thickness, h_*, can be integrated as

$$\frac{\partial h_*}{\partial t} + \nabla \cdot (\mathbf{u}h_*) = B + D_*. \tag{2.2}$$

Note that although h_* satisfies the same equation as h, their initial fields will be different. More importantly, while h and the true velocity are coupled through the momentum equation there is no such coupling for h_*. In this idealized situation, the predicted field h_* is passive in the sense that it is advected by the true velocity, but cannot change the true velocity.

To understand how the predicted field converges to the true field, it is useful to consider the error, $h_e = h_* - h$. From (2.1) and (2.2), h_e satisfies

$$\frac{\partial h_e}{\partial t} + \nabla \cdot (\mathbf{u}h_e) = D_e, \qquad h_e(t = 0) \neq 0, \tag{2.3}$$

where $D_e = D_* - D$.

Assume that D_e takes the form of Laplacian diffusion,

$$D_e = \kappa \nabla^2 h_e,$$

where κ is the (constant) diffusivity coefficient. Multiply (2.3) by h_e and integrate over a closed domain to obtain

$$\frac{1}{2}\frac{\partial}{\partial t}|h_e^2| = -\kappa|\nabla h_e \cdot \nabla h_e| - \frac{1}{2}|h_e^2 \nabla \cdot \mathbf{u}|, \tag{2.4}$$

where

$$|\cdot| = \int (\cdot)\, dx\, dy \Big/ \int dx\, dy.$$

Note that the condition of no normal flow on the boundaries is used in deriving (2.4).

Equation (2.4) gives the time evolution of the norm square of the error, $|h_e^2|$. On the right-hand side, the first term, associated with diffusion, always reduces the norm. The second term, associated with the flow divergence, can either increase or decrease the norm.

Consider a simple case where the divergence term vanishes. Then, the error field h_e satisfies the same equation as for the conserved tracer, τ,

$$\frac{\partial \tau}{\partial t} + \mathbf{u} \cdot \nabla \tau = D. \tag{2.5}$$

Since conserved tracers are homogenized by turbulent flows (Rhines and Young 1983), the error field h_e will also be homogenized. This can be seen from (2.4) where a nonuniform field of h_e can lead to further decrease of the norm square. The eventual uniform value of h_e depends on the initial condition. If the initial condition is such that the total volume in a layer is known, that is, the area integral of h_e is zero at $t = 0$, then the area integral of h_e is zero for all times since the total volume is conserved. This implies that h_e can be homogenized to a uniform zero value, which leads to the convergence of h_* to h. In this case, the process of convergence is analogous to the tracer homogenization.

If the divergence term is not zero, then h_e may not behave exactly like a conserved tracer since the divergence can increase the norm. However, since the flow divergence is associated with ageostrophic flows, it is of order Rossby number smaller than the advective term. Therefore, h_e can still behave like a conserved tracer in the regime where the Rossby number is small. The influence of the flow divergence will be discussed further in later numerical experiments.

b. Convergence timescales

Having argued that the process of error decay is analogous to tracer homogenization, it is natural to expect the timescale for error decay is similar to that for tracer homogenization. The following is a brief description of tracer homogenization.

From Rhines and Young (1983), tracer homogenization is achieved initially by a rapid process of shear disper-

sion, followed by a slow process of diffusion. The rapid phase is when shear enhances mixing *along* streamlines until the tracer reaches an averaged value of the initial tracer along each streamline. For steady flow with large Péclet number $P = LU/\kappa$, where L and U are the length and velocity scales, the rapid phase of shear dispersion occurs over a time of order $T_a = P^{1/3}(L/U)$. For $L = 100$ km, $U = 0.1$ m s^{-1}, and $\kappa = 10$ m^2 s^{-1}, the shear dispersion timescale T_a is about 100 days. This timescale is longer than the advective timescale L/U, which is about 10 days from the above scales. The slow phase of homogenization is when mixing is getting rid of the gradients *across* streamlines. This occurs over a diffusive timescale L^2/κ, typically the order of decades.

Rhines and Young (1983) also discussed the timescales for flows that are oscillatory in time. However, no similar timescales for unsteady flows appear to be available. Nevertheless, since streamlines for such flows are constantly changing, the gradients that initially lay across streamlines may later become realigned along streamlines and can be mixed by shear dispersion. It is likely that the shear dispersion phase can last longer than T_a.

These timescales can be applied to the error decay timescales. Since the slow diffusion takes a timescale of an order of decades, it is less important for assimilation purposes. Also, in reality, inaccuracies in the model and the forcing can contribute to additional errors and so the long-term error decay may not follow the slow diffusive timescale. Thus, for the purpose of this study, the relevant timescale is the shear dispersion timescale when errors are expected to decay rapidly.

In the following, a series of idealized experiments are used to test the hypothesis of error decay by shear dispersion.

3. Model

An isopycnic layer model (Bleck and Smith 1990) is used for the numerical experiments. The momentum and continuity equations are

$$\frac{\partial \mathbf{u}}{\partial t} + \mathbf{u}\cdot\nabla\mathbf{u} + f\mathbf{u}\cdot\mathbf{J} + \nabla M = \mathbf{X}, \tag{3.1}$$

$$\frac{\partial h}{\partial t} + \nabla\cdot(\mathbf{u}h) = B + \kappa\nabla^2 h + D_N, \tag{3.2}$$

where $M = gz + p/\rho$ (g, gravity; p, pressure; and ρ, density) is the Montgomery potential, $\mathbf{J}$ is the matrix that rotates vectors through 90° counterclockwise, $\mathbf{X}$ is the momentum diffusion, and D_N represents the (implicit) numerical diffusion.

The model is a zonally periodic channel. The domain size is 1000 km across the channel, 600 km along the channel, and has a depth $d = 2000$ m. The grid size is 10 km and the baroclinic time step is 1200 s. The Coriolis parameter is a β-plane approximation with $\beta = 2 \times 10^{-11}$ m^{-1} s^{-1} and $f = 0.83 \times 10^{-4}$ s^{-1} at the center of the channel. There are three isopycnic layers with potential density of $\sigma = 27.3$, 27.4, and 27.6 kg m^{-3}. The layer thickness in the top layer varies from 100 m at the northern end to 700 m at the southern end. The middle layer has a uniform 600-m thickness. The Rossby radius of deformation is 30 km, estimated from $\sqrt{[\sigma_1 - \sigma_3]/\rho_0 g d}/f$, where $\rho_0 = 10^3$ kg m^{-3}.

The forcing B is chosen to be only a function of y so that h and h_* can have exactly the same forcing. Figure 1a shows the forcing. It transfers layer thickness at a rate of up to 10^{-5} m s^{-1} from the top layer to the bottom layer on the northern half of the jet and vice versa on the southern half. The middle layer is not forced. The forcing in the bottom layer is opposite to that in the top layer. The flow is baroclinically unstable and the forcing maintains a jet near the center of the channel.

The model was integrated without explicit thickness diffusion (i.e., $\kappa = 0$) for 20 yr. The mean isopycnals averaged temporally and zonally over the last 10 yr are shown in Fig. 1b. The mean zonal velocity ranges from 8 cm s^{-1} in the top layer to 2 cm s^{-1} in the bottom layer (Fig. 1c).

The layer thickness at year 20 is used as the initial field for the predicted layer thickness. All twin experiments consist of running the model again from year 11 to obtain true $\mathbf{u}$ and h. At the same time the predicted layer thickness h_* in each layer is integrated using the true velocity in that layer. All twin experiments are integrated for 720 days and the first day of year 11 is referred to as day 1.

4. Results

a. The case of no explicit diffusion

As the result may be sensitive to numerical diffusion as well as explicit diffusion, it was necessary to demonstrate the influence of numerical diffusion by conducting one twin experiment with no explicit diffusion. This provides a benchmark for later experiments when explicit diffusion is added.

The fields of h and h_* for the top layer at day 0, 60, and 360 are shown in Fig. 2. At day 0, the two fields are considerably different near the center of the channel and almost identical near the boundaries (Fig. 2, left two panels). At day 60, the contours of the predicted field are strongly stretched to create fine filaments and steep gradients. In contrast, this stretching of the layer thickness field is not present in the true field (Fig. 2, middle two panels). Despite the slightly noisy field, it is possible to see that the predicted field has features similar to the true field. Finally, the two fields at day 360 are similar to each other (Fig. 2, right two panels). This shows that the predicted field gradually converges to the true field.

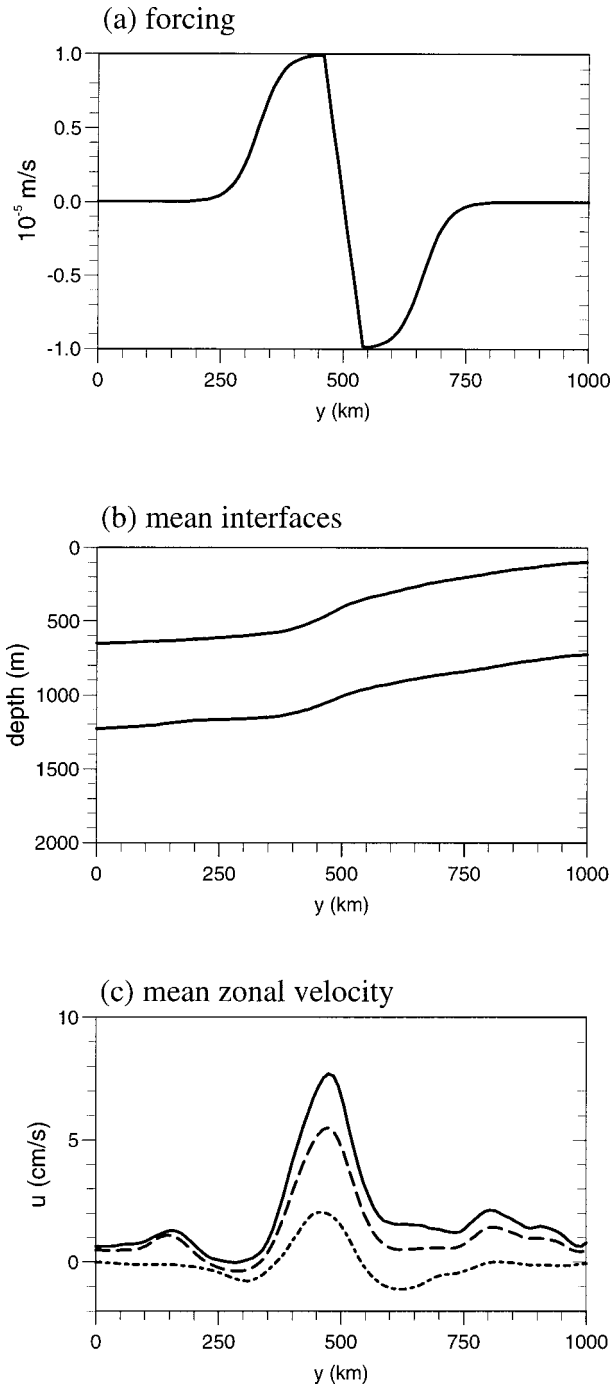

FIG. 1. (a) The forcing function for the top layer. Note that forcing in the middle layer is zero and forcing in the bottom layer is negative of the forcing in the top layer. (b) The mean layer thickness averaged zonally over 10 yr. (c) The mean zonal velocity for the top, middle, and bottom layers, indicated by the solid, broken, and dotted lines.

1) ERRORS DECAY

The convergence can be quantified using the root-mean-square (rms) error, $|h_e^2|^{1/2}$. Figure 3 (solid lines) shows the rms errors for all three layers over the period of 720 days. Both the top and bottom layers show errors decaying fast for the first 100 days, followed by a slow decay. This is similar to the two phases of tracer homogenization as mentioned before.

The middle layer has a different behavior in that the rms error increases first before decreasing. This may be attributed to the flow divergence term discussed in section 2a. To clarify this, two tracers are also integrated but without the divergence term, that is, according to (2.5). One tracer, τ, is initialized as the true h and the other tracer, τ_*, initialized as h_*. The forcing is the same as before. The rms of the tracer error $\tau_e = \tau - \tau_*$, shown in Fig. 3 (broken lines), can be compared to that for the layer thickness.

Over the first 50 days, the two rms errors are similar for the top layer but different for the lower two layers. This may be explained by comparing the advective term ($\mathbf{u} \cdot \nabla h_*$) to the divergence term ($h_* \nabla \cdot \mathbf{u}$) in (2.2). Applying scale analysis to these two terms suggests that the advective term dominates when $\Delta H/H > \Delta U/U$, where Δ is the changes of quantity over a horizontal scale and H is the scale of layer thickness. Given that $\Delta U/U$ is similar in all layers, the advective term dominates when the ratio of the gradient of layer thickness to the layer thickness is large. This ratio is larger in the top layer than in the other two layers. So, including the divergence term makes relatively little difference to the error decay in the top layer compared to the other two layers.

It can also be seen that including flow divergence (in the layer thickness case) has the effect of increasing the errors in the upper two layers but decreasing the errors in the bottom layer. It is not clear why the flow divergence is an error source for the upper two layers and an error sink for the bottom layer.

The comparison between the two rms errors shows that the layer thickness may not behave exactly like a tracer because of the flow divergence. However, the difference between them is small (with the exception of the middle layer) in terms of error decay and so layer thickness can be thought of as a passive tracer.

2) SHEAR DISPERSION

As seen in Fig. 2, the predicted layer thickness field shows closer contours and steeper gradients during the initial error decay. To verify that this is associated with shear dispersion, the time series of the gradients of h_* and h is plotted (Fig. 4). During the first 100 days, the gradients of h_* (heavy solid lines) increase rapidly and then decrease to the values similar to the gradients of true h (light broken lines). The enhanced gradients are the result of shear flow straining the contours of h_* along streamlines so diffusion can take place to get rid of the steep gradients across the streamlines. Therefore, the process of error decay during the first 100 days is shear dispersion.

The efficiency of the error decay may be compared

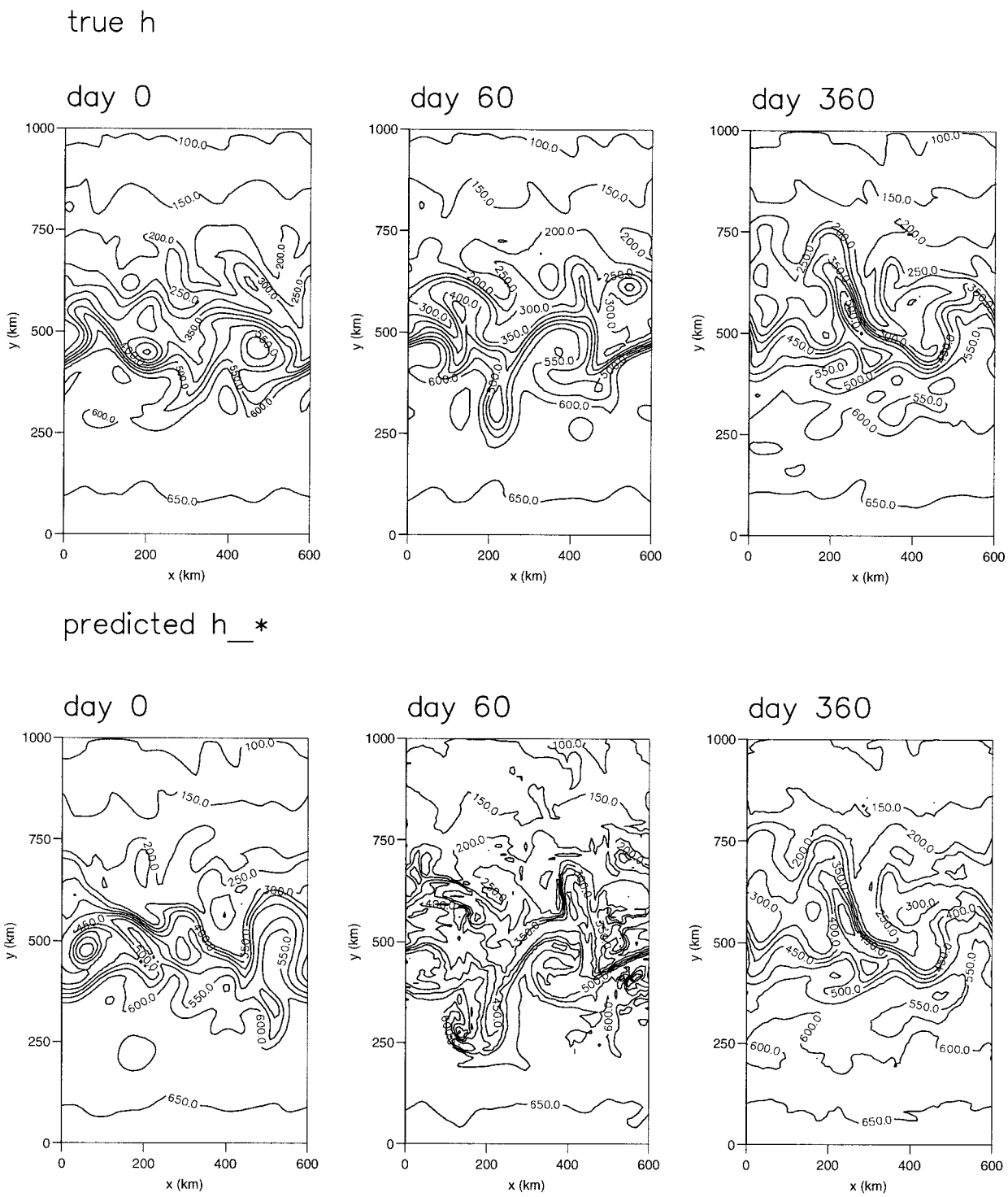

FIG. 2. The layer thickness fields for the top layer at day 0, 60, and 360 (in 50-m contours): the top three panels are the true fields, h, and the bottom three panels are the predicted fields, h_*.

with Haines et al. (1993). The convergence in their experiments is the result of geostrophic adjustment, either through nudging velocity or through constraining potential vorticity in the deep layers. In their case the predicted layer thickness is coupled with the predicted velocity and so geostrophic adjustment occurs when the true velocity is assimilated. This is different from the present experiment in that there is no integration of

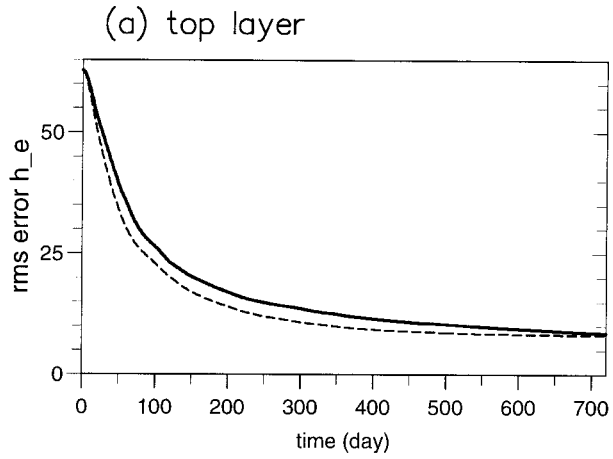

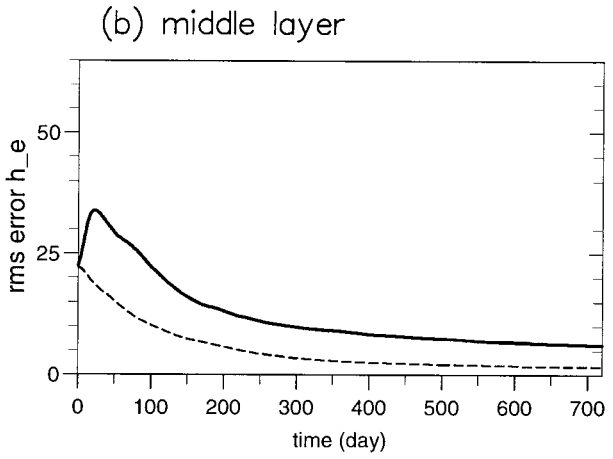

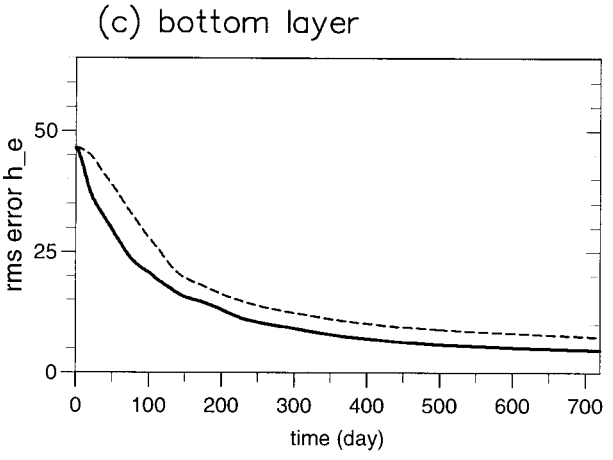

FIG. 3. The time series of rms errors (in m) over 720 days: (a) top, (b) middle, and (c) bottom layer. The solid lines are for the layer thickness, h_e, and broken lines are for the tracer, τ_e.

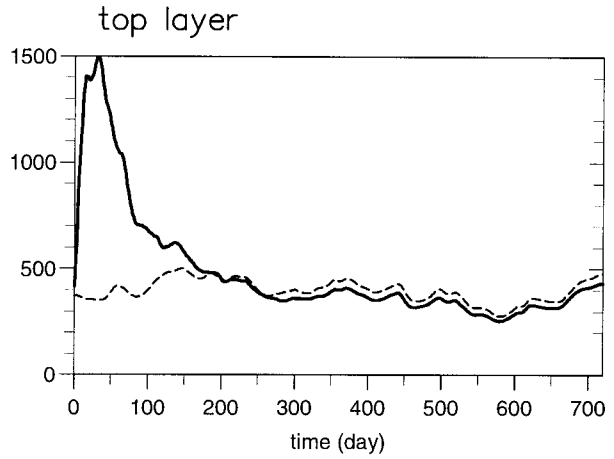

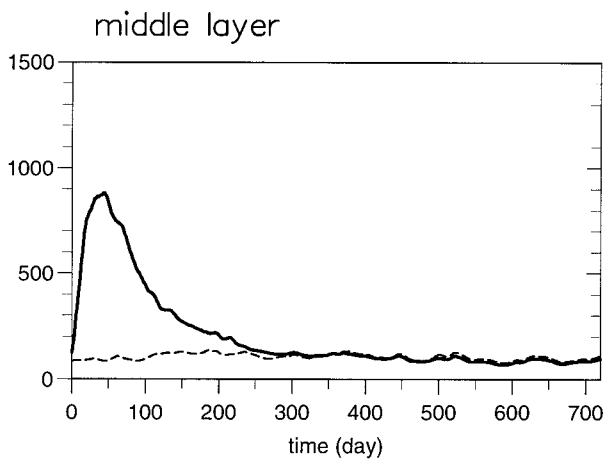

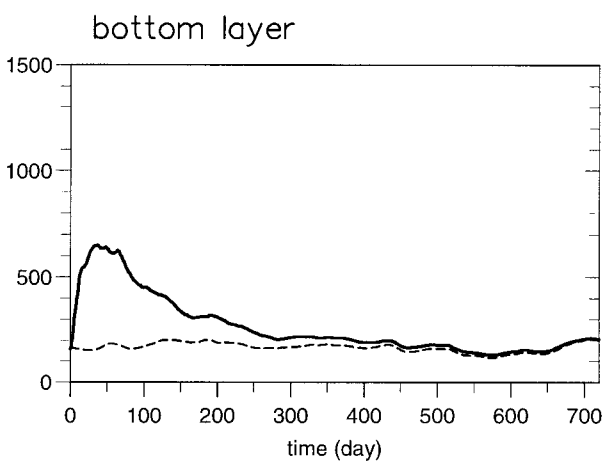

FIG. 4. The time series of gradients in units of 10^{-8} over 720 days. The heavy solid lines are the gradients of the predicted layer thickness, $|\nabla h_* \cdot \nabla h_*|$. The light broken lines are the gradients of the true layer thickness, $|\nabla h \cdot \nabla h|$.

predicted velocity since velocity is assumed perfectly known.

From their Fig. 4g, the rms error for the top-layer thickness is reduced by half after about 10 days whereas in the present experiment the rms error in the top layer is reduced by half after 74 days. This is to be expected as the geostrophic adjustment timescale is of the order of days whereas the shear dispersion timescale is of the order of 10–100 days. In a more realistic assimilation, error decay for layer thickness should be governed by geostrophic adjustment. However, this should not be the case for passive tracers, which have no direct feedback to the velocity. Undoubtedly, passive tracers are advected by a velocity field that contains gravity waves as a result of geostrophic adjustment. However, it seems unlikely that this will cause the error in passive tracers to decay on a geostrophic adjustment timescale. Therefore, shear dispersion could be the significant mechanism.

b. The error decay timescale

So far, the initial decay of rms errors is shown to be associated with shear dispersion. It is reasonable to expect that the decay timescale approximately follows the shear-enhanced diffusive timescale, $T_a = P^{1/3}(L/U)$. The timescale T_a is affected by many parameters including diffusivity in the model. Thus, a series of twin experiments is conducted to test the sensitivity of decay timescales to different diffusivities.

Two points should be made regarding the following experiments. First, as seen earlier, the layer thickness may not converge exactly like a tracer when the flow divergence term becomes important. So the shear dispersion timescale is valid only in the limit when the flow divergence does not influence the error decay too much. Because of this limitation, only the top and bottom layers are suitable for testing the timescale. The results from these two layers are similar qualitatively, so only the top layer will be discussed. Second, although the shear dispersion timescale T_a is for steady flow, it is used here for convenience.

The twin experiments are now conducted with explicit diffusivity added to the integration of h and h_*. Three different diffusivities are tested with $\kappa = 10$, 50, and 100 m^2 s^{-1}.

The time series of the gradients of h_* are shown in Fig. 5a. All three experiments show the enhancement of gradients as seen in the case of no explicit diffusion. As expected, the gradients of h_* decrease when κ increases. However, large diffusivity is only partly balanced by small gradients. For example, when κ increases from 10 to 50 m^2 s^{-1}, the peak gradients of h_* decrease by only about two-thirds. Consequently, diffusion is in fact larger with large diffusivity, implying a faster convergence.

Indeed, the rms errors for the three cases (Fig. 5b) show the errors decrease more rapidly when diffusivity

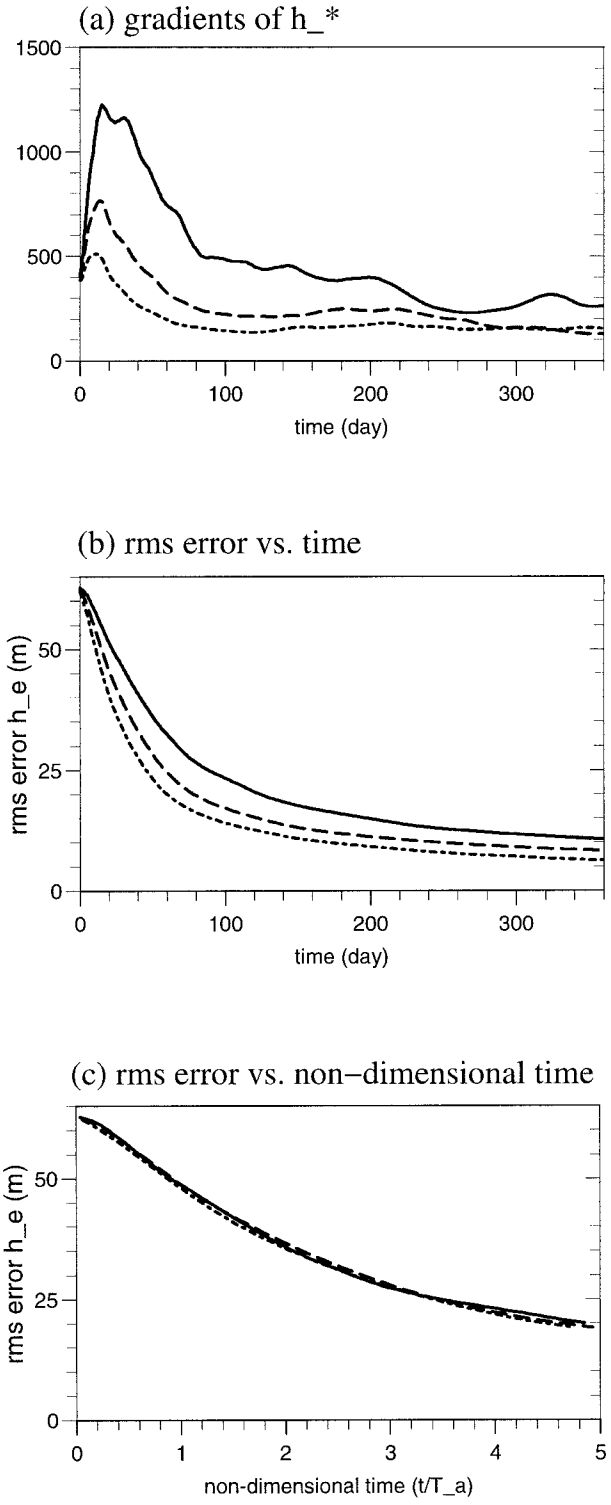

FIG. 5. The solid, broken, and dashed lines indicates the cases with $\kappa = 10$, 50, and 100 m^2 s^{-1}. (a) The time series of the gradients $|\nabla h_* \cdot \nabla h_*|$ in units of 10^{-8} over 360 days. (b) The time series of rms errors (in m) over 360 days. (c) The time series of rms errors plotted against the nondimensional time, t/T_a, where $T_a = 25$, 17, and 14 days for each respective case.

is larger. In the case of $\kappa = 100$ m^2 s^{-1}, the rms error is reduced by half in just 34 days (the dotted line). In other words, the error decay is such that larger diffusivity leads to more efficient shear dispersion and consequently more rapid decay.

The rates of convergence can be rescaled according to the shear dispersion timescale T_a. The contribution from numerical diffusion should be included in the estimate of T_a, as seen earlier that the errors do decay even without explicit diffusion. The form of numerical diffusion is not exactly known, but for convenience it is assumed to be like a Laplacian diffusion. Using (2.4) (ignoring the divergence term) and the rms error from the experiment with no explicit diffusion (Fig. 3a), the numerical diffusivity κ_N is estimated to be about 5 m^2 s^{-1} after averaging over 360 days.

So, the shear dispersion timescale is $T_a = P^{1/3}(L/U) = [(\kappa + \kappa_N)\alpha^2/L^2]^{-1/3}$, where κ_N is the estimated numerical diffusivity and $\alpha = U/L$ is the velocity shear. The length scale L is chosen to be the Rossby radius of deformation, 30 km. The shear α is calculated by averaging $\sqrt{1/2(u_y^2 + v_x^2)}$ over the middle half of the channel for 60 days, which gives $\alpha \sim 0.2$ day^{-1}. These values give shear dispersion timescales $T_a = 25$, 17, and 14 days for each diffusivity. These timescales appear to be the time when the gradients reach their maximum (Fig. 5a), indicating that the scaling is reasonable.

The rms errors are plotted against the nondimensional time, t/T_a, over the period of $5T_a$ (Fig. 5c). The similarity of the three curves confirms that the initial rapid decay timescale follows approximately the shear dispersion timescale. Interestingly, the shear dispersion timescale seems to apply for a period much longer than T_a. This may be due to the fact that the flow is unsteady and streamlines change all the time. So, the contours of constant layer thickness initially lying along streamlines may later become across streamlines, allowing shear dispersion to persist for longer.

5. Discussion

This study examined how the errors in layer thickness decay within the context of twin experiments. Other work has shown that the layer thickness can be recovered by geostrophic adjustment when the velocity field is assimilated using a nudging method (Haines et al. 1993). The question addressed here is to what extent layer thickness can be recovered in the absence of the geostrophic adjustment process. Such a question is relevant to data assimilation as it may serve as a baseline against which assimilation methods can be judged.

The approach is to consider the predicted layer thickness as a passive quantity in the sense that its response to the true velocity is through advection, and, in particular, no feedback of the predicted layer thickness to the true velocity is allowed. In this setting, it was argued that the process of error decay is analogous to tracer homogenization.

Two processes occur during tracer homogenization—an initial rapid shear dispersion, followed by a slower diffusion (Rhines and Young 1983). A similar phenomenon is also observed in the convergence of layer thickness where error decays rapidly at first and then decays slowly. However, the timescales are such that only the initial rapid decay is important for the purposes of assimilation.

The initial rapid decay of errors is associated with enhanced gradients and therefore shear dispersion. Further experiments with different diffusivities show that the timescales for initial rapid decay approximately follow the shear dispersion timescales, $T_a = P^{1/3}(L/U)$.

The similarity between tracer homogenization and error decay holds as long as the flow divergence term does not dominate over the advection term. In the present model, the flow divergence term affects the middle layer in such a way that the rms error increases initially rather than decreasing.

In summary, the study shows shear dispersion as a mechanism for decaying errors. This may be compared to geostrophic adjustment. First of all, the shear dispersion timescale (order of 10–100 days) is longer than the adjustment timescale (order of days). In terms of recovering layer thickness in a more realistic assimilation, geostrophic adjustment will be the dominant process. However, in terms of passive tracers, it is unlikely that these will be recovered on the geostrophic adjustment timescale because of the lack of feedback of tracers to velocity.

It is commonly accepted in the assimilation community that the predicted tracer field loses the memory of the initial condition on the advective timescale. This timescale is, in general, longer than geostrophic adjustment. However, the prediction still has to converge to the truth over some timescale. This study shows that this timescale is likely to be the shear dispersion timescale, which is generally longer than the advective timescale.

Throughout the study, perfect knowledge of velocity and forcing is assumed. Although these assumptions are common in twin experiments, they are rarely satisfied in real data assimilation. In reality, there are difficulties such as imperfect models, poorly known forcing, and inadequate data. Despite the difference between real assimilation and twin experiments, there is still much to be learned from twin experiments where convergence processes can be identified, helping to understand what might be going on in the real assimilation.

Acknowledgments. This study was funded by the EU MAST-2 program, DYNAMO CT930060. I thank George Nurser, Peter Killworth, and Keith Haines for helpful discussions, and Rainer Bleck and Linda Smith for providing the numerical code. I also thank the anonymous referees for helpful suggestions.

REFERENCES

Berry, P. J., and J. C. Marshall, 1989: Ocean modelling studies in support of altimetry. *Dyn. Atmos. Oceans,* **13,** 269–300.

Bleck, R., and L. T. Smith, 1990: A wind-driven isopycnic coordinate model of the North and equatorial Atlantic Ocean. I. Model development and supporting experiments. *J. Geophys. Res.,* **95,** 3273–3285.

Haines, K., 1991: A direct method for assimilating sea surface height data into ocean models with adjustments to the deep circulation. *J. Phys. Oceanogr.,* **21,** 843–868.

——, P. Malanotte-Rizzoli, R. E. Young, and W. R. Holland, 1993: A comparison of two methods for the assimilation of altimeter data into a shallow-water model. *Dyn. Atmos. Oceans,* **17,** 89–133.

Rhines, P. B., and W. R. Young, 1983: How rapidly is a passive scalar mixed within closed streamlines? *J. Fluid Mech.,* **133,** 133–145.